Study of removal characteristics of anionic and cationic metals using poly(methacrylic acid) grafted mesoporous natural zeolite

Seo-Hyun Pak, Hwan Kim, Chan-gyu Park*

*Environmental Technology Division, Korea Testing Laboratory, 87, Digital-ro 26-gil, Guro-gu, Seoul 08389, Korea,
Tel. +82 02 860 1105; Fax: 82-02-860-1689; email: pcg6189@hotmail.com (C.-G. Park), Tel. +82 2-860-1139; Fax: +82 2-860-1689;
email: seohyunpak@ktl.re.kr (S.-H. Pak), Tel. +82 2-860-1258; Fax: +82 2-860-1689; email: hhwany@ktl.re.kr (H. Kim)*

ABSTRACT

Polymerized mesoporous nature zeolites (pMNZ) were simply prepared by acid treatment and polymerization of metallic acid, which evaluated as adsorbents for the removal of cationic/anionic heavy metals from aqueous solutions. The effects of treatment time and different acids during synthesis on the pore structure of the mesoporous nature zeolites (MNZ) were studied, and the pMNZ samples were characterized by nitrogen full isotherms, X-ray fluorescence analysis, and Fourier-transform infrared spectroscopy. The MNZ prepared using hydrochloric acid had higher mesopore volume and surface area. The Brunauer–Emmett–Teller analysis showed that the surface area of MNZ is 82 m^2 g^{-1} greater than that of natural zeolite that is 39 m^2 g^{-1}. We investigated the adsorption ability of pMNZ for metal ions (Cu(II), Mn(II), and As(V)) and evaluated the influence of pH. The removal efficiencies of pMNZ for Cu(II), Mn(II), As(V) were 44%, 51%, 99% and q_e were 0.88, 0.75, 0.04, respectively. In addition, the adsorption kinetics were evaluated using pseudo-first-order and pseudo-second-order models. The internal and external diffusion models were studied to explain the adsorption process in pMNZ. The adsorption capacity resulted that the pMNZ could eliminate the anionic, cationic metal ions from aqueous solution at a pH range of 6–10 and different kinetics were examined to explain the adsorption process.

Keywords: Grafting polymerization; Mesoporous natural zeolite; Water treatment; Toxic pollutants; Cationic/anionic metals and metalloids

1. Introduction

Abnormalities frequently occur in which toxic contaminants are generated in major water systems due to increasing temperatures and environmental pollution caused by global climate change. Importantly, continuous exposure to metals and metalloids (Cd, Mn, Hg, Cu, and As) is harmful to human beings, animals, and plants [1–4]. In addition, consumer's expectations for high-quality drinking water are increasing, and thus drinking water is becoming more thoroughly monitored by stricter inspection.

Extensive research on water purification methods such as micro-filtration, ultra-filtration, nano-filtration, adsorption (activated carbon), and ion-exchange membranes [5–8] has been performed. However, there remains a need for new treatment processes that can overcome the limitations of existing methods. To overcome these limitations, various nanomaterials have been modified to develop adsorbents with high functionality and selectivity, and new adsorbent materials have been developed, such as ion-exchange resins, mesoporous materials, and graphene. Among these new adsorbents, mesoporous-based materials have been applied in various applications [9] due to their high surface areas and pore structures.

* Corresponding author.

Natural zeolites are crystalline aluminosilicates consisting of a skeleton of tetrahedral molecules and have unique activities, low costs, and adsorption capacities for heavy metals, nitrates, phosphates, and organic pollutants in wastewater [10,11]. However, the micropores of zeolites cause issues regarding restricted transport due to diffusional limitations. The mesopores created in natural zeolites enhance the diffusion rate by improving the access of substrates to micropores and shortening the diffusion path length [12]. The economical and simple methods for the generation and growth of pores in natural zeolite have been reported by some workers.

For example, Ates et al. [13] studied the effect of alkali treatment on the characteristics of natural zeolites and showed that the method increased the mesostructures, surface area, and adsorption capacity for Mn^{2+} (164.5 mg g^{-1}). Wang et al. [14] reported a basic treatment in natural clinoptilolite for the improvement of zeolite physicochemical properties, and Burris and Juenger [15] studied the effect of acid treatment on the reactivity of natural zeolites used as supplementary cementitious materials.

The polymerization of zeolite has gained interest on account of the low costs, high stability, and affinity towards the target metals. Mainly, various polymers with zeolites and mesoporous materials have been investigated as adsorbents for the removal of heavy metals [16]. Roque et al. [17] reported pyrrole oligomerization within zeolite channels, and Shin et al. [18] reported the structure of poly (ethylene terephthalate)/A-zeolite nanocomposites [18].

Herein, we present a simple process to synthesize micro/mesoporous natural zeolite (mesoporous ratio > 50%) via desilication/dealumination with HCl of natural zeolite, polymerized zeolite with methacrylic acid and applied the polymerized zeolite as an adsorbent. The mesoporous nature zeolites (MNZ) were characterized by nitrogen full isotherms and X-ray fluorescence (XRF) analysis, and the polymerized mesoporous nature zeolites with poly(methacrylic acid) (pMNZ) were characterized by Fourier-transform infrared spectroscopy. The removal capacity of pMNZ for Cu(II), Mn(II), and As(V) from wastewater was also studied. This work demonstrates a material with significant potential for the removal of both anionic and cationic metals from water.

2. Materials and methods

2.1. Chemicals

Natural zeolite (clinoptilolite, Si/Al = 4, size: 3 mm) in gravel form was purchased from Geumnong Industrial at Korea. Hydrochloric acid (HCl) was purchased from Samchun Chemical (Korea) and used without purification. Sodium hydroxide (NaOH, 0.1 M) and ammonium chloride were purchased from Sigma-Aldrich (USA).

The reagents used for the iron-oxide coating and polymerization of zeolite were purchased from Sigma-Aldrich (USA), and methacrylic acid (MA), sodium persulfate ($Na_2S_2O_8$), and sodium metabisulfite ($Na_2S_2O_5$) were used without further purification. Mn(II)·SO_4 and Cu(II) Cl_2 were obtained from Samchun Chemical (Korea), and arsenate (As(V)) was prepared from sodium arsenate dibasic heptahydrate (Sigma-Aldrich, USA).

2.2. Syntheses

To prepare MNZ, the natural zeolite was washed and dried at 105°C for 1 d before use. Then, 5 g of the natural zeolite was added to 6 mL of hydrochloric acid and mixed for 180 min at 90°C. Subsequently, the zeolite was washed with distilled water, and the remaining material was dried at 105°C for 2 h to yield the MNZ. For iron-oxide coating, 20 g of MNZ was added to a 500 mL aqueous solution of 20% $FeCl_3$ (≥99.99%) and mixed for 60 min at 150°C. Subsequently, the water was removed using a vacuum distiller. The material was calcined at 250°C for 2 h to produce iron-oxide MNZ.

To synthesize pMNZ, MA (5 mL, 99%) was added to 95 mL of deionized water in a beaker. Then, initiators were added (weight ratio S_2O_5/S_2O_8 = 0.6), and the MA, initiators, and iron-oxide MNZ (5 g) were mixed at room temperature. After 30 min, the product was washed with deionized water, and the obtained sample was denoted as pMNZ. An illustration of the pMNZ is shown in Fig. 1.

2.3. Batch sorption studies

Batch sorption experiments were performed on the adsorbent with 50 mL of metal solutions containing Mn(II), Cu(II), and As(V) at room temperature. Metal solutions were prepared to dissolve an accurate amount of metal salts. And pH was adjusted by the drop-wise addition of 0.1 N of HCl and NaOH solutions. Adsorbent (0.5 g) was mixed with the metal solution (50 mL), and samples were obtained at different time intervals. The concentrations of the manganese and copper solutions were analyzed by UV/vis spectroscopy (Hach, DR 5000, USA) using standard methods (Mn: periodate oxidation method, Cu: method 8506 (CuVer 1)) for examining the water. The concentration of arsenic was determined by inductively coupled plasma measurements (ICP, VARIAN 730ES, Australia). The q_e was calculated by the following equation:

$$q_e = \frac{V(C_0 - C_t)}{w} \tag{1}$$

where q_e is adsorbed amount at time t (mg g^{-1}), C_0 is the initial concentration (mg L^{-1}), C_t is the liquid concentration at time t (mg L^{-1}), V is the volume of the solution (L), and w is the weight of the adsorbent (g).

2.4. Analysis methods

Nitrogen (N_2) full isotherms were measured at 77 K by an ASAP 2020 analyzer (Micromeritics, USA). The surface area of the sample was calculated using the Brunauer–Emmett–Teller (BET) method, and the pore size distribution was determined using the non-local density functional theory method (NLDFT). The organic functional groups were characterized by attenuated total reflection–Fourier-transform infrared spectroscopy (ATR–FTIR; Nicolet spectrophotometer 5700, Thermo Scientific, MA) with a ZnSe crystal at an incident angle of 45°. The elemental compositions of the samples were determined by X-ray fluorescence spectrometry (XRF, S4 PIONEER, Germany) at the National Instrumentation Center for Environmental Management (NICEM) at Seoul National University.
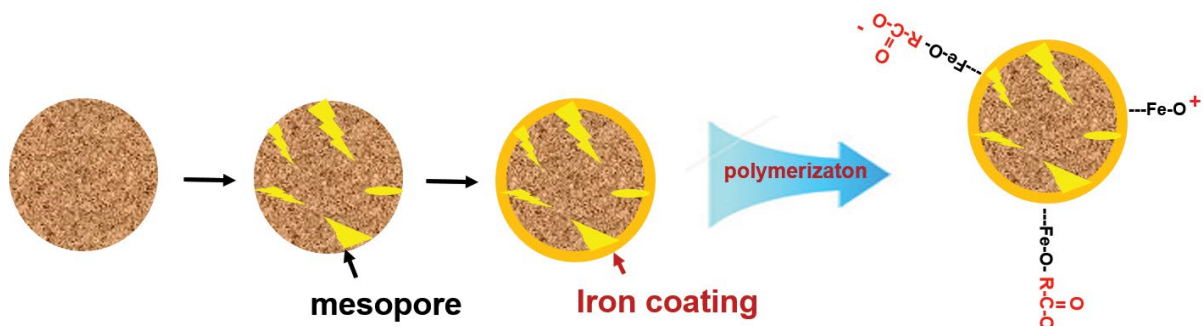
Fig. 1. Schematic diagram of polymerized mesoporous natural zeolite.

3. Results and discussion

3.1. Characterization of pMNZ

The pMNZ was prepared by treatment with hydrochloric acid, iron-oxide coating, and polymerization with MA, and the material was analyzed by N_2 adsorption–desorption isotherms, XRF, and ATR–FTIR spectroscopy. Nitrogen full isotherms were collected to determine the differences between the surface areas of the natural zeolite (NZ) and MNZ. The nitrogen adsorption isotherms for the treated NZ samples prepared under different synthesis conditions are shown in Fig. 2 and Table 1.

The isotherms of MNZ-1 and MNZ-3 are typical IV type isotherms indicating mesopore sorption behavior. All isotherms clearly indicate a steep condensation step at $P/P_0 = 0.4$–0.6. The broader hysteresis loop and H4 hysteresis type of MNZ-3 suggest slit-like pores, irregular shapes, and broad size distribution of mesopores. Furthermore, the surface area (Table 1) of most samples increased upon acid treatment of the natural zeolite because the acid treatment causes dealumination and desilication. The samples were sensitive to the effects of treatment time and acid type. The surface area of MNZ-3 is lower than that of MNZ-2, but the ratio of the mesopore volume of MNZ-3 (Table 1) is the highest among the samples (mesoporous ratio > 50%). The results show that mesopores were formed via decomposition of the natural zeolite by strong acid (HCl) for 3 h. When the processing time exceeded 6 h, the existing pores collapsed, resulting in irregular macropore volumes.

The elemental compositions and amount of iron oxide were identified by XRF analysis and are presented as the percentage of each element's highest oxidation state
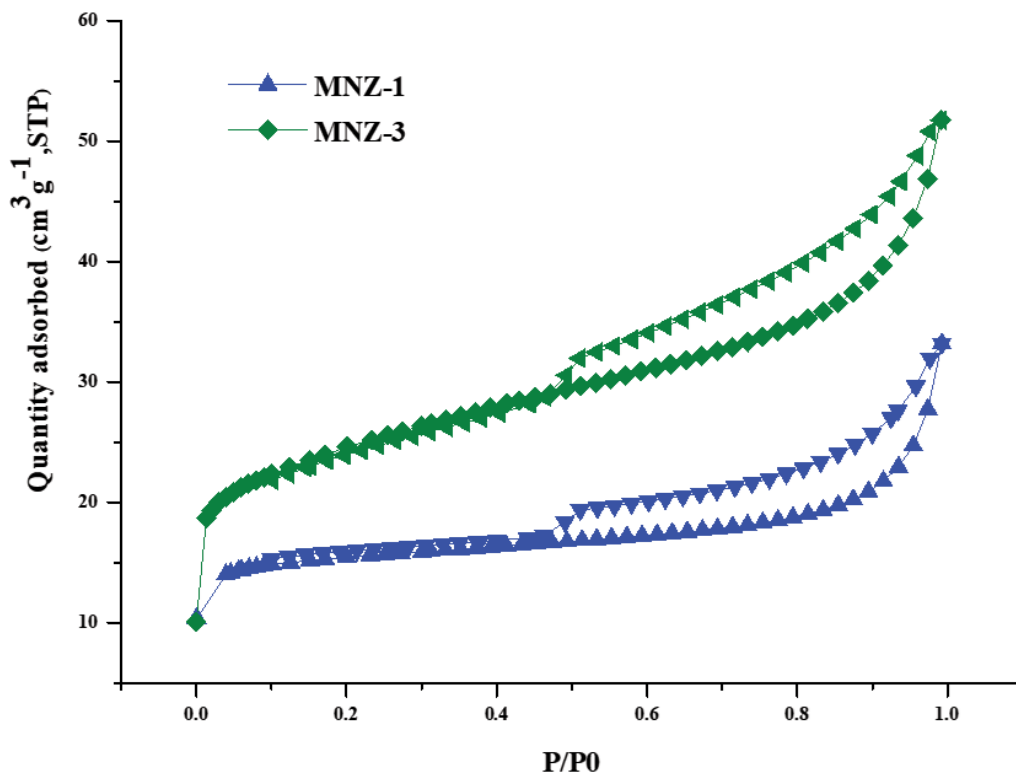
Fig. 2. The N_2 adsorption–desorption isotherms of the samples with different kinds of acid and reaction times.

Table 1
Textural properties of the samples prepared with a different kind of acid and reaction times

	BET surface area	Total pore volume	DFT pore volume (<2 nm)	DFT pore volume (2–50 nm)	DFT pore volume (50 nm)	Mesopore volume ratio (%)
	$m^2\,g^{-1}$	$cm^3\,g^{-1}$	$cm^3\,g^{-1}$	$cm^3\,g^{-1}$	$cm^3\,g^{-1}$	
NZ	39	0.052	0.011	0.017	0.024	32
MNZ-1 (HNO$_3$, 6N, 3 h)	49	0.049	0.017	0.010	0.022	20
MNZ-2 (HNO$_3$, 6N, 6 h)	87	0.083	0.018	0.017	0.048	20
MNZ-3 (HCl, 6N, 3 h)	82	0.080	0.024	0.041	0.015	51.25
MNZ-4 (HCl, 6N, 6 h)	81	0.076	0.018	0.010	0.048	13.15

(Table 2). The iron percentage in MNZ was 5.6%. The higher amount of Fe_2O_3 in iron oxide MNZ than in NZ indicated that iron oxide was successfully doped onto the MNZ. The minor amounts of other elements from natural zeolite also contained (Ru, Mn, Sr, Cu, and so on).

The ATR–FTIR analysis results of NZ, MNZ, and pMNZ are illustrated in Fig. 3. The spectra were recorded in two regions: 4,000–1,280 cm^{-1}, where the ~3,400 cm^{-1} band represents –OH, which was reduced in intensity due to desilication and delamination after hydrochloric acid treatment; and 1,280–700 cm^{-1}, where the band at 1,000 cm^{-1} is characteristic of zeolite. This band shifted from 1,000 to 1,033 cm^{-1} due to desilication and delamination (Figs. 3a and 3b). Fig. 3c shows the significantly different results obtained from MNZ-3, indicating the formation of carboxylic acid bonds and the presence of certain functional groups on the iron-oxide-coated zeolite surface after modification. The bands at 1,696 and 3,201 cm^{-1} correspond to –C=O and –OH group stretching vibrations, and the bands at 1,640 and 1,387 cm^{-1} are assigned to the γ_s(COO$^-$) and asymmetric γ_{as}(COO$^-$) modes, respectively [19,20]. In addition, the peak at 1,486 cm^{-1} is assigned to δ(–CH$_2$).

3.2. Adsorption of Cu(II), Mn(II) and As(V)

Fig. 4 exhibits the adsorption trend of the pMNZ depending on the initial pH. The pollutant solution (50 mL, 4 ppm Mn C_0, 2 ppm Cu C_0) was mixed with the adsorbent (0.5 g pMNZ, 100 rpm). The Mn(II) concentration of the solution with pMNZ adsorbent changed from 4 to approximately 1.7 mg L^{-1} over 4 h. Thus, the maximum removal percentage toward Mn(II) of pMNZ (4 h) was 57.5%, which is a charged solute at pH 9. In addition, the maximum removal percentage toward Cu(II) of pMNZ was 44.0% at pH 9. This indicated that the cationic heavy metal adsorption ability of pMNZ is pH-dependent. Below pH 7, carboxyl groups are not charged because they are protonated,

and the coated iron ions on pMNZ are positively charged. When the adsorption of Cu(II) and Mn(II) is carried out at pH 7 or less, the adsorbent and adsorbate are both positively charged, and thus the adsorption does not proceed. Above pH 7, both the functional groups and coated iron ions are anionic, which facilitates the adsorption of cationic heavy metals. pMNZ has a similar affinity for Mn(II) ions compared to Cu(II) ions. However, as the surface of the pMNZ becomes negatively charged, the active sites showed a greater affinity for Mn(II) ions.

The adsorption of Cu(II), Mn(II), and As(V) was tested using the NZ and pMNZ at room temperature and a contact time of 240 min at initial Cu(II), Mn(II), and As(V) concentrations of 4, 2, and 0.03 mg L^{-1}, respectively (Fig. 5). Experiments were carried out to investigate the influence of the mesoporous ratio on metal adsorption. As shown in Fig. 5, the removal efficiencies of NZ, pMNZ for Cu(II) were 36%, 44%, and q_e of NZ, pMNZ were 0.72, 0.88, respectively. And the removal efficiencies of NZ, pMNZ for Mn(II) were 25%, 51% and q_e of NZ, pMNZ were 0.42, 0.75, respectively. The carboxylic acid groups and mesoporosity of the pMNZ increased the adsorption capacity for Mn(II), Cu(II). The highest removal ratio was 99% for As(V) and q_e was 0.04, which is a charged solute at pH 7; As(V) is negatively charged in the pH range between 4 and 10.

The large surface area of pMNZ allows for the generation of more active sorption sites for the modification of iron oxides. Furthermore, the adsorption efficiency is improved by coating iron oxide on the high-surface-area pMNZ, which acts as a cation exchange resin.

3.3. Adsorption kinetics

To compare the adsorption rate and completion time of the adsorbent, a kinetic experiment was conducted, and the C/C_0 results with time are shown in Fig. 6. In order to identify an effective kinetic model for the adsorption process,

Table 2
Chemical analysis of natural zeolite (NZ) and iron modified zeolite (iron oxide MNZ)

Constituent (wt.%)	Al_2O_3	SiO_2	CaO	MgO	Fe_2O_3	LOI[a]
NZ	10.3	45.7	2.39	0.88	1.8	33.3
Iron oxide MNZ	8.42	45.6	1.2	0.61	5.6	33.3

[a]Loss on ignition
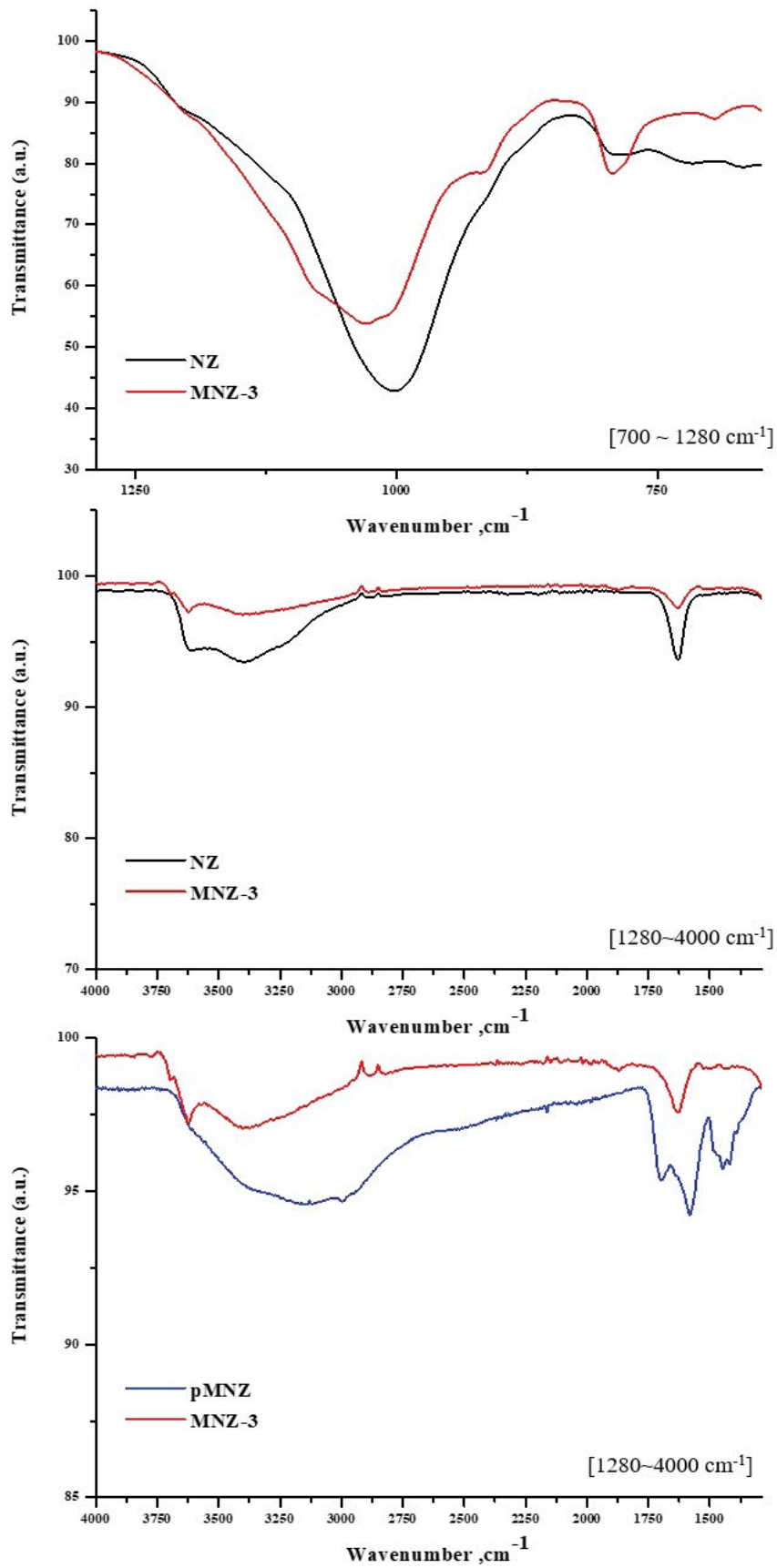
Fig. 3. ATR–FTIR spectra for the natural zeolite (NZ), MNZ-3, and pMNZ.
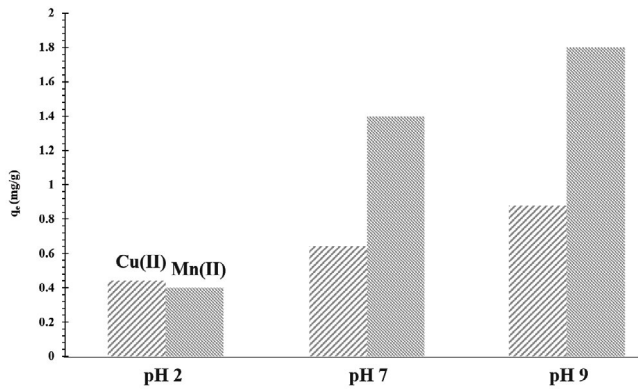
Fig. 4. Effect of pH on Cu(II) and Mn(II) removal using pMNZ.
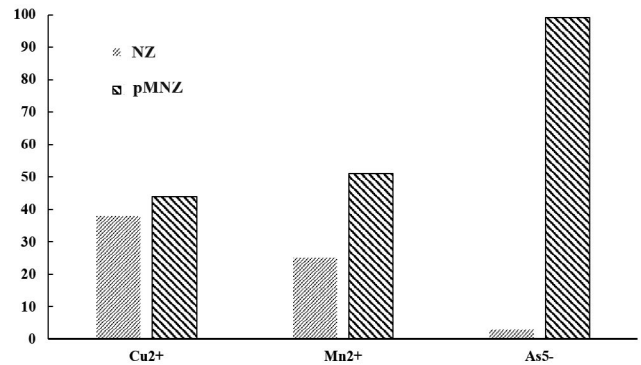
Fig. 5. Comparison of removal ratio (%) of heavy metal ions by NZ and pMNZ.
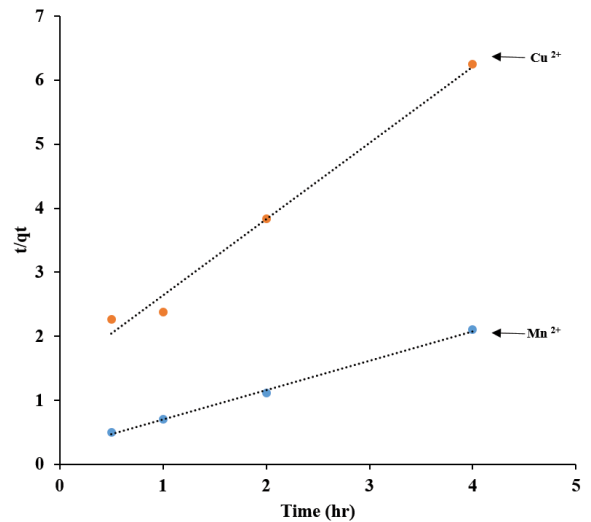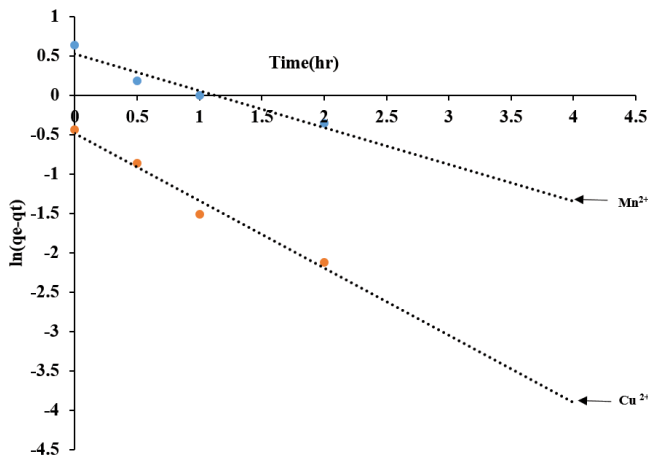
Fig. 6. (a) Pseudo-first-order and (b) pseudo-second-order kinetic fits of Mn(II), Cu(II) by pMNZ. [TS: Kindly label the parts as (a) and (b)]

an understanding of calculations for typical kinetic models is required. The kinetic models for this analysis included pseudo-first-order (PFO) and pseudo-second-order (PSO) models [21]. Based on the results in Fig. 5, the PFO and PSO models were fitted to the adsorption isotherms, and the adsorption constants obtained from the isotherms are given in Table 3.

The PFO equation is one of the most common for modeling the sorption of solutes from aqueous solutions:

$$\frac{dq}{dt} = K_{ad}\left(q_e - q_t\right), \tag{2}$$

where K_{ad} is the reaction rate constant, q_e is the adsorbed amount at equilibrium (mg g^{-1}), q_t is the adsorbed amount at reaction time t (mg g^{-1}), and t is time (min). The above equation can be re-expressed as follows:

$$\ln\left(q_e - q_t\right) = \ln q_e - K_1 t \tag{3}$$

The PSO kinetics is based on the adsorption equilibrium capacity of the solid phase and are described as below:

$$\frac{dq}{dt} = K_2\left(q_e - q_t\right)^2 \tag{4}$$

where K_2 is the reaction rate constant.

The calculated adsorption rates using the PFO and PSO kinetic models shown in Fig. 6 indicate that the adsorption rates of pMNZ are high regardless of the metal type. From the data in Table 3, the calculated q_e value for the PSO model is similar to the experimental value with a high correlation coefficient. The PSO model of pMNZ did provide a good fit for the experimental data as can be seen from the high regression (R^2) values of 0.99 and 0.98 for Mn(II) and Cu(II) ions, respectively [22,23]. Thus, the kinetics of the adsorption of Mn(II) and Cu(II) onto pMNZ can be explained adequately by the PSO kinetic model.

3.4. External and internal diffusion models

The removal rate of adsorbate is determined by the mass transfer rate, and the diffusion path of an adsorbate can be classified as external diffusion or internal diffusion.

Table 3
Correlation coefficients between measured and predicted data

Metal	q_e (exp.) (mg g^{-1})	First-order			Second-order		
		K_{ad} (h^{-1})	q_e (theor.)	R^2	K_2 (g mg^{-1} h^{-1})	q_e (theor.)	R^2
Mn^{2+}	1.9	0.47	1.7	0.94	0.98	2.18	0.99
Cu^{2+}	0.64	0.85	0.6	0.97	2.4	0.841	0.98

Table 4
Parameters of the internal and external diffusion model for adsorption of Mn^{2+} onto the natural zeolite (NZ) and polymerized mesoporous natural zeolite (pMNZ)

Methods	Adsorbent	$k_s \times 10^{-7}$	R^2
External diffusion	NZ	0.12	0.99
	pMNZ	0.60	0.96
		k_{id}	R^2
Internal diffusion	NZ	0.069	0.88
	pMNZ	0.119	0.99

The external diffusion model, also known as the film diffusion model, was suggested by Spahn and Schlünder and is defined as follows [24]:

$$v \frac{dC}{dt} = -k_s A \left(C - C_s \right) \tag{5}$$

which can be applied by modifying to

$$-\ln \frac{C}{C_0} = k_s \frac{A}{V} t \tag{6}$$

where k_s is the mass transfer coefficient (m^2 s^{-1}), C is the concentration of adsorbate in solution (mg L^{-1}), C_s is the adsorbate concentration at the surface of the adsorbent (mg g^{-1}), A is the surface area of the adsorbent (m^2), v is the volume of the solution, and t is time (s).

The adsorption rate of Mn(II) to pMNZ is faster than to NZ because the mesoporosity increases the material transfer speed; the material is also more reactive to cationic heavy metals.

The internal diffusion model was proposed by Weber and Morris [25] and is defined as follows:

$$q_t = C + k_{id} t^{1/2}, \tag{7}$$

where q_t is the adsorption rate (mg g^{-1}) at time t, k_{id} is the diffusion rate in the pores, t is time (min), and C is related to the thickness of the boundary layer. The results of the adsorption test were applied to the internal diffusion model (Fig. 7). The internal diffusion rate was lower than the external diffusion rate, and because pMNZ also developed internal pores, contaminants were constantly removed during the experiment. Thus, the internal diffusion rate varied minimally during the experimental period.
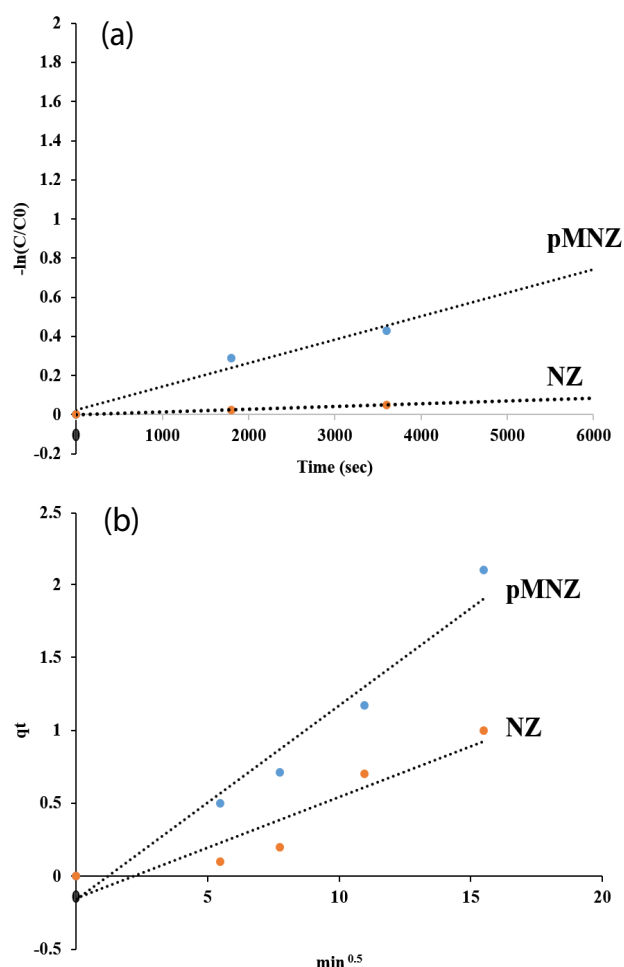
Fig. 7. Plot of (a) external and (b) internal diffusion model for adsorption of Mn(II) onto the natural zeolite (NZ) and meso-natural zeolite (pMNZ).

4. Conclusions

The purpose of this study was to investigate the characteristic of adsorption on pMNZ and evaluate the removal efficiency of heavy metals through batch tests. The adsorption results were analyzed using the PFO and PSO models to evaluate the kinetic properties of the pMNZ. The carboxylic acid groups and mesoporosity of the pMNZ increased its adsorption capacity for Mn(II), Cu(II), and As(V). The pMNZ showed promising potential for the removal of both anionic and cationic metals from water and can be further tested at a pilot scale.

Symbols

A —   Adsorbent surface area, m^2

C_0 —   Initial concentration, mg L^{-1}

C_s —   Adsorbate concentration at adsorbent surface, mg L^{-1}

C_t —   Concentration at time t, mg L^{-1}

K_2 —   PSO rate constant

K_{ad} —   PFO rate constant

k_{id} —   Pore diffusion rate

k_s —   Mass transfer coefficient, $m^2\,s^{-1}$

q_e —   Adsorbed amount at equilibrium, mg g^{-1}

q_t —   Adsorbed amount at time t, mg g^{-1}

V —   Sample volume, L

w —   Adsorbent weight, g

References

[1] R. Costanza, R. d'Arge, R. de Groot, S. Farber, M. Grasso, B. Hannon, K. Limburg, S. Naeem, R.V. O'Neill, J. Paruelo, R.G. Raskin, P. Sutton, M. van den Belt, The value of the world's ecosystem services and natural capital, Nature, 387 (1997) 253.

[2] P. Roccaro, C. Barone, G. Mancini, F.G.A. Vagliasindi, Removal of manganese from water supplies intended for human consumption: a case study, Desalination, 210 (2007) 205–214.

[3] I.J. Lee, K.-L. Lee, T.-H. Lim, J.-J. Park, S. Cheon, Determination of geosmin and 2-MIB in Nakdong River using headspace solid phase microextraction and GC-MS, J. Anal. Sci. Technol., 26 (2013) 326–332.

[4] S.B. Watson, Aquatic taste and odor: a primary signal of drinking-water integrity, J. Toxicol. Environ. Health Part A, 67 (2004) 1779–1795.

[5] D. Ellis, C. Bouchard, G. Lantagne, Removal of iron and manganese from groundwater by oxidation and microfiltration, Desalination, 130 (2000) 255–264.

[6] A. Alpatova, S. Verbych, M. Bryk, R. Nigmatullin, N. Hilal, Ultrafiltration of water containing natural organic matter: heavy metal removing in the hybrid complexation–ultrafiltration process, Sep. Purif. Technol., 40 (2004) 155–162.

[7] B.A.M. Al-Rashdi, D.J. Johnson, N. Hilal, Removal of heavy metal ions by nanofiltration, Desalination, 315 (2013) 2–17.

[8] S.B. Wang, Y.L. Peng, Natural zeolites as effective adsorbents in water and wastewater treatment, Chem. Eng. J., 156 (2010) 11–24.

[9] P.W. Seo, J.Y. Song, S.H. Jhung, Adsorptive removal of hazardous organics from water with metal-organic frameworks, Appl. Chem. Eng., 27 (2016) 358–365.

[10] W.H. Zou, H.J. Bai, L. Zhao, K. Li, R.P. Han, Characterization and properties of zeolite as an adsorbent for removal of uranium(VI) from solution in fixed bed column, J. Radioanal. Nucl. Chem., 288 (2011) 779–788.

[11] K. Margeta, N.Z. Logar, M. Šiljeg, A. Farkas, Natural Zeolites in Water Treatment – How Effective is Their Use, W. Elshorbagy, R.K. Chowdhury, Water Treatment, InTechOpen, (2013) 81–112, doi: 10.5772/50738.

[12] A. Balati, A. Shahbazi, M.M. Amini, S.H. Hashemi, K. Jadidi, Comparison of the efficiency of mesoporous silicas as absorbents for removing naphthalene from contaminated water, Eur. J. Environ. Sci., 4 (2014) 69–75.

[13] A. Ates, Effect of alkali-treatment on the characteristics of natural zeolites with different compositions, J. Colloid Interface Sci., 523 (2018) 266–281.

[14] C. Wang, S.Z. Leng, H.D. Guo, L.Y. Cao, J.F. Huang, Acid and alkali treatments for regulation of hydrophilicity/ hydrophobicity of natural zeolite, Appl. Surf. Sci., 478 (2019) 319–326.

[15] L.E. Burris, M.C.G. Juenger, The effect of acid treatment on the reactivity of natural zeolites used as supplementary cementitious materials, Cem. Concr. Res., 79 (2016) 185–193.

[16] S.-H. Pak, S.-M. Park, J. An, C.-g. Park, Adsorption behavior of poly(methacrylic acid)/iron-oxide-coated zeolite for the removal of Mn(II), Fe(II), and As(III) from aqueous solution, Desal. Water Treat., 123 (2018) 150–155.

[17] R. Roque, J. de Onate, E. Reguera, E. Navarro, Pyrrole oligomerization within H-Fe-FAU zeolite, J. Mater. Sci. Lett., 12 (1993) 1037.

[18] Y.H. Shin, W.D. Lee, S.S. Im, Effect of A-zeolite on the crystallization behavior of in-situ polymerized poly(ethylene terephthalate) (PET) nanocomposites, Macromol. Res., 15 (2007) 662–670.

[19] S. Karimi, J. Feizy, F. Mehrjo, M. Farrokhnia, Detection and quantification of food colorant adulteration in saffron sample using chemometric analysis of FT-IR spectra, RSC Adv., 6 (2016) 23085–23093.

[20] A. Drmota, A. Košak, A. Znidaršič, A mechanism for the adsorption of carboxylic acids onto the surface of magnetic nanoparticles, Mater. Technol., 42 (2008) 79–83.

[21] Y.S. Ho, G. McKay, The kinetics of sorption of basic dyes from aqueous solution by sphagnum moss peat, Can. J. Chem. Eng., 76 (1998) 822–827.

[22] B. Das, N.K. Mondal, Calcareous soil as a new adsorbent to remove lead from aqueous solution: equilibrium, kinetic and thermodynamic study, Univ. J. Environ. Res. Technol., 1 (2011) 515–530.

[23] M.A.O. Badmus, T.O.K. Audu, B.U. Anyata, Removal of lead ion from industrial wastewaters by activated carbon prepared from periwinkle shells, Turk. J. Eng. Environ. Sci., 31 (2007) 251–263.

[24] H. Spahn, U. Schlünder, The scale-up of activated carbon columns for water purification, based on results from batch tests—I: theoretical and experimental determination of adsorption rates of single organic solutes in batch tests, Chem. Eng. Sci., 30 (1975) 529–537.

[25] W.J. Weber, J.C. Morris, Kinetics of adsorption on carbon from solution, J. Sanitary Eng. Div., 89 (1963) 31–38.